Iranian Journal of Chemical Engineering
Vol. 12, No. 1 (Winter 2015), IAChE

Hydrodynamic Characteristics of Dense Conical Fluidized Bed: CFD Simulation and Experimental Verification

A. R. Bahramian

Department of Chemical Engineering, Hamedan University of Technology, Hamedan, Iran

Abstract

The hydrodynamic characteristics of dense conical fluidized bed were investigated experimentally and numerically. Experimental studies have been carried out in a bed containing TiO_2 particles belonging to A/C boundary of Geldart's classification with a wide particle size distribution. Pressure measurements and an optical fiber technique allowed determining the effect of high bed particles loading on the minimum fluidization velocity, local solid volume fraction and solid velocity. Two-fluid model approach with three different drag models and boundary conditions (BCs) consisting of no-slip, partial-slip and free-slip BC is presented for the numerical predictions. In this paper, we show the Gidaspow drag function with k-ε turbulent model by applying the partial-slip BC can improve the numerical results at high particle loading.

Keywords: *Dense flow, Micrometric Particles, Conical Fluidized Bed, Particles Loadings, Numerical Approach*

1. Introduction

Dense particle-fluid flows are frequently encountered in a variety of industrial units, of which the conical fluidized bed can be mentioned as an important example. Owing to suitable fluidization characteristics of conical beds such as their ability to handle coarse particles and cyclic flow patterns, these beds are often applied in the chemical, petrochemical and pharmaceutical industries, and catalytic polymerization in large dimensions [1-4]. Conical beds are also an alternative to fluidization of high loading of wet or cohesive particles with wide size distribution in a hot medium to more drying efficiency and particle segregation.

The main problem in studying conical beds is the complex motions of gas and particles, where the interaction between two phases is unknown. Many independent variables such as size, shape and density of particles, bed voidage, gas and particle velocity and type of flow regime significantly affect the hydrodynamics behavior of these beds. For particles smaller than 100 μm, cohesive forces are significant. Zhou and Li [5] studied the fluidization of fine powders and determined that some particles should be fluidized when gas velocities are in excess of their apparent

∗ Corresponding author: bahramian@hut.ac.ir

minimum fluidization velocities. This is due to fact that these Geldart-C particles form agglomerates during fluidization. Researches showed that self-agglomeration could be beneficial to the fluidization process in displaying a hydrodynamic behavior similar to that of Geldart-A particles and proposed a modified Geldart's diagram with A/C and A/B boundaries [6-7]. Various experimental techniques such as dynamic pressure fluctuations, laser-Doppler anemometry adopted with refractive index matching scheme, and optical fiber probe have been used to measure the bed hydrodynamic parameters, the solid volume fraction and particle velocity [1,8-10].

In recent years, to arrive at a better understanding of bed hydrodynamics of fluidized beds, numerical approaches have become a suitable way [11-12]. In the literature, computational fluid dynamics (CFD) method has been used for modeling of two phase flow. This method consists of two parts: a Lagrangian-Eulerian approach (Trajectory model) for updating the velocities and positions of the particles from the Newtonian's law, and an Eulerian-Eulerian approach (Two-fluid model) for updating the local gas density and velocity from the Navier-Stokes equation. The advantage of two-fluid model is that it can account for the particle-wall and particle-particle interactions in a realistic manner, for system containing micrometric particles. The kinetic theory of granular flow (KTGF) is used in the two-fluid model to describe the particulate phase stress through constitutive equations. For this model in the dilute phase, particles fluctuate randomly; this form of viscous dissipation and stress is called kinetic stress, while in the dense phase, particles can collide briefly, giving rise to further dissipation and stress, known as collisional stress. At high dense phases with high particles loading (more than 50% by volume fraction), grains undergo large sliding and rubbing contacts, leading to a different form of dissipation and stress, called frictional stress.

It is important to calculate the hydrodynamic characteristics of bed containing poly-dispersed particles. Mostafa simulated two-phase flow in a fluidized bed with different particles size by using two-fluid model [13]. Particles were classified into several zones according to their diameter and each zone was treated as a phase with certain velocity. His simulated results were in good agreement with measurements using laser doppler velocimetry (LDV) technique. Bahramian and Olazar have used two-fluid model with kinetic theory of granular flow in CFD simulation of micrometric particles in a conical fluidized bed [14]. The simulated results were in good agreement with measurements using optical fiber technique. Based on this, they obtained relevant information concerning minimum fluidization velocity, solid volume fraction and solid velocity in a conical fluidized bed with relatively low particle loadings. However, they observed significant errors between the predicted bed expansion ratio and the experimental observation utilizing different drag models. Van Wachem *et al*. [15] studied the effects of different drag models on hydrodynamics behavior of fluidized beds. They found that the values of the pressure drop, bed expansion and bubble diameter, which was proposed by Syamlal-O'Brien drag model were in better agreement with

experimental data in comparison with other drag models, while Almuttahar and Tagiphour [16] reported no significant difference in hydrodynamic behavior of a two-dimensional fluidized bed of Geldart-B particles using different drag model. Van Wachem *et al*. [15] also reported that the kind of slip condition imposed at the wall is not critical in simulation of bubbling fluidized bed whereas Bahramian *et al*. [16] show the boundary conditions (BCs) play an important role in simulation of micrometric particles in a conical fluidized bed. Benyahia *et al*. [17] used the free slip BC at the wall in their simulations. They used semi-empirically-derived boundary conditions in the CFD models proposed by Johnson and Jackson [18].

Two limits due to low and high friction effect were investigated in the solid phase for estimating the collision of solid particles with the wall, thereby predicting a core-annulus flow. Their results show that a high friction boundary condition causes unrealistically large granular energy production at the wall. Almuttahar and Taghipour [16] applied BCs developed by Johnson and Jackson [18] in their simulation of a circulating fluidized bed riser. They reported that the choice of different slip conditions, corresponding to free- or no-slip BCs, affects the solid behavior of FCC particles near the riser wall. Hosseini *et al*. [19] used similar slip conditions in CFD simulation of circulation-fluidized bed. Their results showed that utilizing the boundary condition of Johnson and Jackson that accounts for the partial slip of the solid particles at the walls could be suitable for simulation of the solid hold-up distribution of the bed. Bahramian *et al*. [20] show the choice of BC has different results in determination of hydrodynamic parameters in a conical fluidized bed. They found that the use of the partial-slip BC in the simulations gives a lower value of mean standard deviation in the determination of the minimum fluidization velocity than when using the free- or no-slip BC. However, the results obtained for bed expansion ratio using the free-slip BC are slightly better than those obtained by implementing the Gidaspow model with the other BCs.

The main goal of the present study is fluidization characteristics of micrometric particles in a conical fluidized bed with dense flow, while hydrodynamic characteristics of dilute flow were studied in the previous works. In this work, the minimum fluidization velocity, radial profiles of solid volume fraction and solid velocity were determined by optical fiber technique and CFD simulation in high particle loadings of lab-scale conical fluidized bed unit containing poly-dispersed dried TiO_2 particles. The performance of the Eulerian-Eulerian approach with the kinetic theory of granular flow and three different drag models, consisting of Gidaspow [21], Syamlal-O'Brien [22] and Arastoopour [23] functions, and BCs, corresponding to no-slip with friction, partial-slip with partial-friction, and free-slip without friction BCs were evaluated by comparing their predictions with our experimental results.

2. Experimental procedure

The experiments have been carried out in a lab-scale conical fluidized bed unit (STREA-1, Niro-Aeromatic Co.). This unit is geometrically similar to the industrial-scale one used in the petrochemical and

pharmaceutical industries. The gas distributor is a porous stainless plate. Dry air has been used as the fluidizing gas; its flow rate has been controlled with a ball flow meter. The experimental apparatus and its dimensions are shown schematically in Fig. 1. Experiments have been performed to identify the steady state bed pressure drop at different superficial air velocities, U_a, from 0 to 1.40 m/s. Optical experiments and digital treatment were carried out by the Laser and Optic Research School of Iran. A dual function optical probe was used to measure local particle volume fraction and local particle velocity simultaneously. An intrusive fiber optic probe capable of measuring the local particle velocity and the local solid volume fraction in a conical bed was tested. The probe was first used to measure the particle velocity of poly-dispersed TiO_2 particles and a calibration procedure was then developed in order to calibrate the probe for the measurement of the local solid volume fraction of particles. A fiber-optic probe method is applied to determine the mean solid volume fraction and particle velocity at different zones. An Nd-YAG laser is used as a light source with a frequency of 50 Hz. A 12 V light source transmits light to the emitting fiber. The light signal is collected by photodiodes and converted into voltage (1-100 mV). The signals then pass through the amplifier (-12 to +12 V). An analogue/digital interface sends the reflected light data to the computer for processing. Detailed discussions of the measurement techniques are provided in our previous studies [1,4,14 and 20].

The particles used throughout this experiment are dried titanium dioxide (TiO_2) particles with a range of diameters of 90 to 600 μm belonging to A/C boundary in the Geldart's classification diagram [24]. Two different particles loading, H_o, corresponding to 0.08 and 0.10 m have been used in the experiments. The physical properties of TiO_2 particles are given in Table 1. The size distribution of the TiO_2 particles used in this study is given in Table 2.

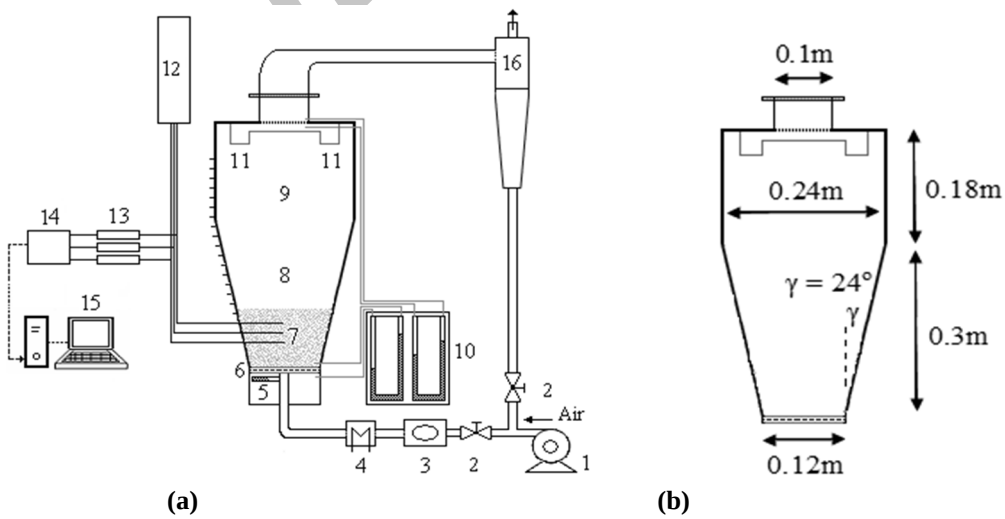

(a) **(b)**

Figure 1. (A) Experimental apparatus: 1. Air compressor, 2. Valves, 3. Rotameter, 4. Electrical clement, 5. Probe thermometer, 6. Gas distributor, 7. TiO_2 particles, 8. Conical section, 9. Cylindrical section, 10. Manometers, 11. Filters, 12. Light source, 13. Detectors, 14. Amplifier, 15. Computer and monitoring, 16. Cyclone; (B) Dimensions of vessel.

Table 1
Physical properties of TiO_2 particles used in this study.

Property	Symbol (unit)	Value	
Average particle size	$d_{p,\,avg}$ (μm)	300	
Particle density	ρ_p (kg/m^3)	4500	
Bulk density	$_b\rho$	H_o (m)	ρ_b (kg/m^3)
		0.08	123
		0.10	12
Maximum packing limit	$\alpha_{s,max}$	0.89	

Table 2
Particle size distribution of the powder used.

Sieve opening, d_{pi} (μm)	Weight fraction, x_i	$(x/d_p)_i$	$d_{p,avg}$ (μm)
90-106	8.96×10^{-2}	5.88×10^{-4}	95
106-125	2.92×10^{-2}	1.54×10^{-4}	108
125-200	2.70×10^{-1}	1.45×10^{-3}	163
200-250	1.47×10^{-1}	4.49×10^{-4}	225
250-300	1.14×10^{-1}	3.03×10^{-4}	275
300-355	5.96×10^{-2}	1.37×10^{-4}	328
355-400	2.79×10^{-1}	4.86×10^{-4}	378
400-600	1.24×10^{-2}	1.91×10^{-5}	500
Total	1	3.58×10^{-3}	300

2-1. Governing equations

The Eulerian-Eulerian approach (two-fluid model) with KTGF and k-ε turbulence model has been used in all simulations (see Appendix A). In this model, both gas and particulate phases are considered as a continuum and a set of Reynolds-averaged conservation equations for the mass and momentum of both phases, gas kinetic energy of turbulence and its dissipation can be written in a generic transport form. The governing and constitutive equations for both the gas and particulate phase are solved sequentially at each iteration to obtain the dependent hydrodynamics variables (see Appendix B).

2-2. Numerical procedure

The numerical procedure used here is given as follows:

(a) The two-dimensional cylindrical or coordinate system can be chosen.

(b) Since the hydrodynamics parameters such as solid volume fractions and velocities of micrometric particles with wide size distributions are not needed to be known for engineering purposes, a simpler means for calculating the mean particle diameter is required. By using the mean diameter of 300 μm, instead of the various different sizes of the particles (from a range of 90 to 600 μm), the simulation of a poly-dispersed bed can be simplified to that of a mono-sized system.

(c) Pressure and velocity are treated as the main variables. The velocities have been solved by coupling the two phases in a segregated state and the pressure equation was built based on the total volume continuity rather than mass continuity. Pressure-velocity coupling has been achieved by using the phase coupled SIMPLEC algorithm.

(d) The governing equations have been solved by the finite control volume technique. The momentum equations are discretized by First order upwind (FOU) scheme. The full implicit formulation for all terms was used to derive the discretization equations.

(e) The mesh density with a grid size of 208×50 was used in the CFD simulation. This mesh has been chosen to fulfill the conditions for near-wall function and to minimize the solution's dependence on mesh density.

(f) The time step in unsteady simulations has been varied from 5×10^{-5} to 1×10^{-3} s, depending on the solution convergence. The time step automatically decreases when the solution is changing more rapidly, and it increases when fast transients subside in order to minimize computation time. The computation time for simulating 6 seconds of real time was approximately 25 hours on a PC with a 3.2 GHz Pentium 4 CPU.

(g) The mean particle diameter is used in the simulation because the difficulty of simulating the flow of a poly-dispersed material. Because of the very large number of particle collisions in the dense phase flow, it could be considered that particles with different sizes had the same average velocity.

2-3. Boundary conditions

The boundary conditions used here are given as follows:

(a) z=0 (Inlet), the Dirichlet BC is used to specify a uniform linear gas velocity, U_g, i.e., 0.1, 0.5, 1.0 and 1.4 m/s. The inlet solid velocity is zero.

(b) z=0.485 m (outlet), the velocity gradients for the two phases is zero. Furthermore, the pressure is set as atmospheric condition.

(c) r=0 (center), symmetrical boundary condition is applied.

(d) r=R (wall), no-slip BC is used for the gas phase, whereas three types of specularity coefficients, φ, are used for the solid phase. Based on this, Schaeffer [25] approach was applied for no-slip BC (φ=1.0), whereas semi-empirical equations developed by Johnson and Jackson [18] are used for free-slip (φ=0) and partial-slip (φ=0.5) BCs. (see Appendix C).

(e) At the outlet, the pressure is specified (atmospheric condition).

3. Results and discussions

Figs. 2-3a show the experimental data and simulation results of evolution of pressure drop relative to superficial air velocity for two particles loading of 0.08 and 0.1 m. This figure is usually called characteristic curve which was mentioned in the previous studies [1,3,5,7,12 and 14]. The experimental observations show that at high particles loading, when applying low air velocities (below 0.5 m/s), TiO_2 particles tend to stick to each other and to the walls even in low moisture content in which local inter particle capillary and weight forces cause particle agglomeration, especially in the bottom of the bed. The ratio of inter particle force to weight force is defined as the granular Bond number,

Bo_g in some literature [7]. In this condition, the pressure drop values were much higher than the bed with low particles loading, as a result the bed is in a fixed state. The pressure drop gradually rose with increasing air velocity until at velocities corresponding to U_g=0.5 m/s. The air passes through particles with formation of large bubbles and bed slowly obtains a wave-like structure caused by air slits traveling from the cone bottom section along the vessel axis until the motion of particles finally starts at the minimum fluidization velocity, U_{mf}. It can be seen from Figs. 2-3a, when particles loading increased from 0.08 to 0.10 m, the minimum fluidization velocity changed from about 0.34 to 0.415 m/s, respectively.

The increase in the minimum fluidization velocity caused by the conical vessel containing particles loading of 0.08 m allows higher superficial air velocities and higher flow dissipation rates than high particles loading of 0.1 m. When particles loading is increased from 0.08 m to 0.10 m the peak pressure drop increases from 1.12 to 1.21 kPa, respectively. Also, with increase of the particles loading, the greater part of gas flow passes through the axial zone in the central bed section while the annulus in the lateral section are less penetrated by the flow. As a result, high pressure drop represents the bed reaction to the gas flow because TiO_2 particles tend to stick together and to the wall.

Before further discussions on the complex behavior of the bed at high particles loading, the effect of the particles loading on the flow regime must be discussed. At low particles loading (especially in $H_o \leq 0.024$ m), it could be shown that the transition region is fairly undistinguished and bed pressure drop is balanced with the weight of the particle per unit area, therefore, low superficial air velocities are enough for bed to reach full fluidization state [3,11]. Increase in the particles loading makes the transitions more easily detectable since we get a deep bed with sections showing different fluidization behavior. In this case, the bed pressure drop is lower than the bed weight, suggesting that the bed is in a heterogeneous fluidization state.

By increasing air velocity to about 0.74 (Fig. 2a) and 0.83 m/s (Fig. 3a), at particles loading of 0.08 and 0.1 m, respectively, the channels gradually break up and fluidization turns from heterogeneous to uniform fluid-like type, which means that the bed is in a homogenous fluidization state. At high air velocities, corresponding to $U_g > 0.9$ m/s, the air simply passes through the bed without any significant effect on pressure drop which is referred to as full fluidization state. The velocity that describes the bed behavior in this state is called the complete fluidization velocity, U_{cf} (Figs. 2-3 a).

The pressure drop above the weight of the particles per unit area is called overpressure in the literature [11,19]. The overpressure enables simultaneous breaking of the bonding between the particles and the distributor plate. After full fluidization, the experiments showed that the overpressure maintains constant values of 0.48, 0.52 and 0.71 kPa, when the particles loading was 0.012, 0.024 and 0.050 m, respectively, While at high particles loading corresponds to 0.08 and 0.1 m, pressure drop remains constant around 0.86 and 0.92 kPa, respectively. It suggests that the adhesion between the particles, particle-wall friction and contact between particles with gas distributor is important in

determination of pressure drop at high particles loading and dense flows.

Fig. 2b shows the simulated pressure drop values across the bed as a function of gas velocity. Three different types of drag function, Gidaspow [21], Syamlal-O'Brien [22], and Arastoopour [23] were applied to obtain the simulated values (See Appendix D).

According to the experimental observation, two main mixing mechanisms in conical fluidized bed can be identified: (1) convective transport and mixing, which is caused by the solid circulation and play a leading role in the particle mixing, especially in the axial mixing; (2) diffusive mixing, which takes place among solid circulation, mainly responsible for the radial mixing. Based on the above mixing mechanism, the effect of particles loading on the particle mixing can be explained. Comparison of axial and radial solid velocity shows that axial mixing is far faster than radial mixing [1,11]. Thus, the axial mixing mechanism affects the top and bottom of fluidized bed much more significantly than the radial mixing in the conical fluidized bed.

A comparison between the experimental data and the simulation results shows that the transition region including heterogeneous and homogenous state is unclear in all simulations. Also, the values obtained from simulations are lower than the experimental data; because of the cohesive nature of TiO_2 particles, a certain accumulation of particles is observed and causes a delay in fluidization of TiO_2 particles. It was found that using the drag models of Syamlal-O'Brien [22] and Arastoopour [23] leads to lowering the pressure drop compared with the Gidaspow model. The mean standard deviations between Syamlal-O'Brien, Arastoopour and Gidaspow drag models with the experimental data were 15.7%, 14.1% and 12.2%, respectively, for particles loading of 0.08 m. Therefore, Gidaspow [21] drag model appeared to be the most suitable for the wide range of gas velocities.

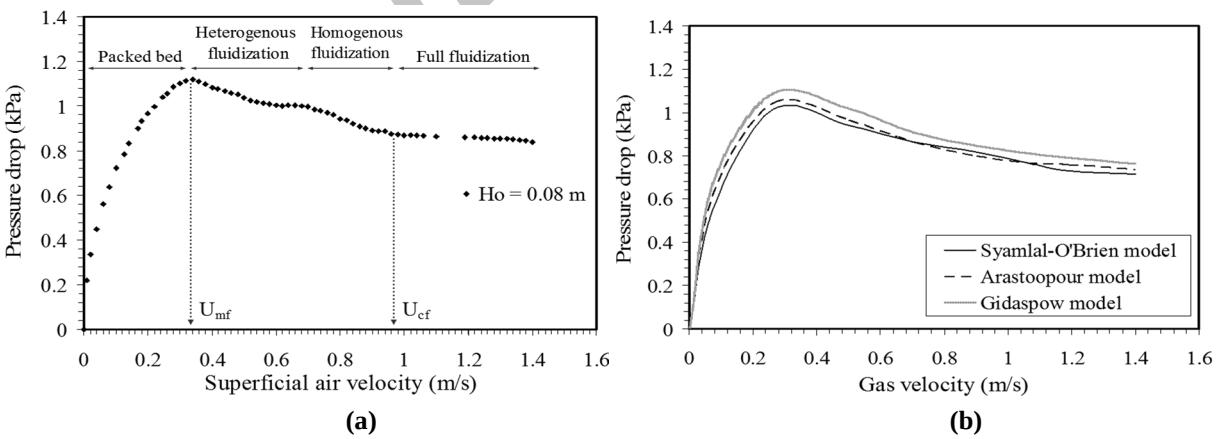

Figure 2. Characteristic curve (Pressure drop-Air velocity) of H_o=0.08 m.
(a) Experimental data, (b) Simulation results of drag models.

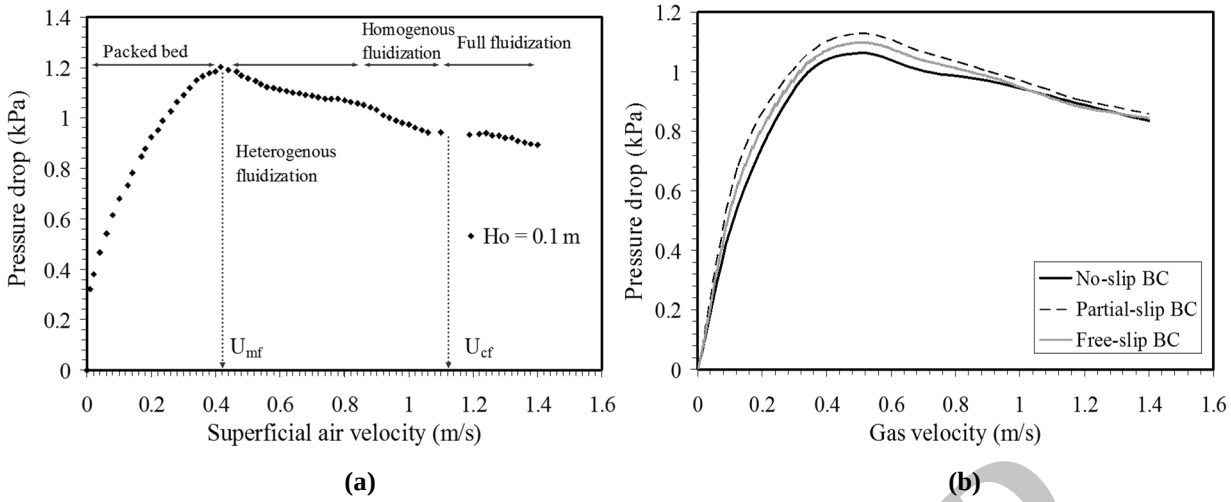

(a) **(b)**

Figure 3. Characteristic curve (Pressure drop-Air velocity) of H_o=0.10 m. (a) Experimental data, (b) Simulation results of boundary conditions.

Fig. 3b shows the simulated pressure drop as a function of gas velocity when three different boundary conditions consisting of no-, partial- and free-slip BCs is imposed using Gidaspow drag model [21]. It is found that using the partial-slip BC leads to higher pressure drop than the other BCs. The mean standard deviations between no-slip, partial-slip and free-slip with the experimental data were 16.4%, 11.1% and 12.9%, respectively, for particles loading of 0.10 m. Thus, partial-slip BC showed better agreement than the other slip conditions.

Fig. 4 shows qualitative snapshots of the bed solid volume fraction with different air velocities, corresponding to 0.1, 0.5, 1.0, and 1.4 m/s obtained by using the Gidaspow [33] drag model and applying partial-slip BC and a restitution coefficient, e_{ss}, of 0.9. These solid volume fraction contours correspond to 6.0 s after starting to introduce the gas into the bed when particles loading was 0.10 m. Fig. 4a corresponds to an air velocity below minimum fluidization velocity, U_g=0.1 m/s. The flow patterns of solid particles at low air velocities in high loads of conical fluidized bed are similar to the spouted bed [1,4]. At low particles loading of conical fluid bed, when low air velocity is applied, the bed attains a wave-like structure because of air bubbles traveling from the bottom to the top of the bed [20]. Although at high particles loading particles descend slowly at the walls which is called the annulus zone, much higher particle velocities are obtained in the center of the bed, namely spout zone. Fig. 4b shows the gas velocities corresponding to above the minimum fluidization velocity (U_g=0.5 m/s). In this state, some channels exist in the bed. Gas passes through these channels until the channels gradually disrupt and fluidization occurs at the central region of the bed. When the inlet gas velocity further increases to 1.0 m/s (Fig. 4c), the height of bed expansion increases and finally, at high air velocity corresponding to 1.4 m/s (Fig. 4d), the gas passes through the bed without forming a spout and annular zones and fairly full fluidization occurred. By comparing the present results with our previous study for

relatively low particles loading, it can be found that at high particles loading, there is a clear distinction between the annular and spout zones, with low bed volume fraction in the spout zone and a sharp change at the spout-annulus interface. In annulus, where particles are in close contact with each other, the bed volume fraction is relatively uniform and almost equal to the initial packed bed (see Fig. 4d).

Fig. 5a and b shows the radial dimensionless distribution curves of mean solid volume fraction in a conical fluidized bed for the particles loading of 0.08 m, with an inlet air velocity of 1.0 (Fig. 5a) and 1.4 m/s (Fig. 5b). In these figures, z denotes the axial direction from the bottom of the vessel. Experimental data and simulated results obtained by the Gidaspow [21] drag model and applying partial-slip BC show that the solid volume fraction is low in the spout zone and high in the annular zone. The mean solid volume fraction decreases in the spout and annular zones as the bed height are increased. It should be noted that the mean solid volume fraction does drop directly to minimum value in the spout zone ($-0.05 \leq r/R \leq 0.05$) while in annular zone ($-0.28 > r/R$, $0.28 < r/R$), where particles are in close contact with each other, the bed volume fraction is fairly uniform and almost equal to the initial packed bed. As observed in Fig. 5, the maximum value of the mean solid volume fraction at z=0.05 m decreases roughly from 0.62 to below 0.1 and 0.5 to below 0.1, when air velocity is increased from 1.0 to 1.4 m/s, respectively. Moreover, as shown in Fig. 5, it may be concluded that the curves are asymmetrical at the radial directions. This asymmetrical behavior means that apart from the bed vertical flow, there is another type of solid circulation on the vicinity of the walls, which is called gulf-effect in the literature. This phenomenon was observed in the experimental data and simulation results of conical fluidized bed, but scant attention has been paid to this phenomenon in the simulations of other researchers who undertook experimental works only [11,15,16].

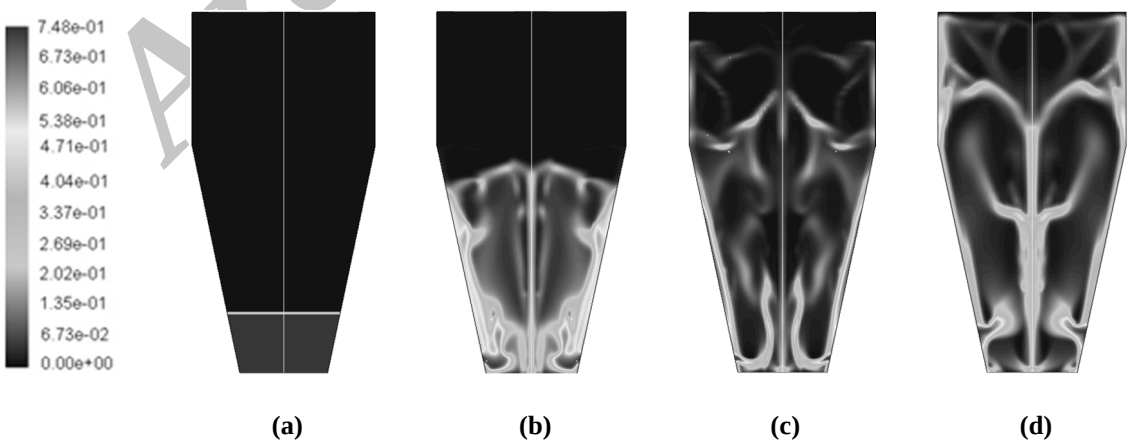

Figure 4. 2-D Simulated distribution of solid volume fraction profile. (a-d) Gidaspow model, Partial-slip BC, e_{ss}=0.9, H_o=0.10 m, t=6 s [(a) 0.1, (b) 0.5, (c) 1.0, (d) 1.4 m/s]

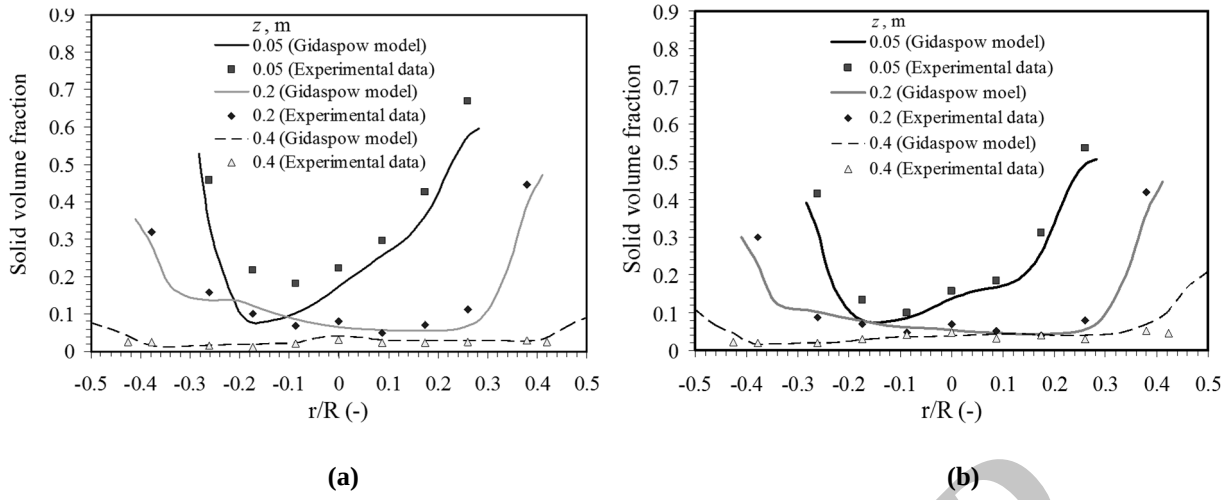

Figure 5. Radial distribution of solid volume fraction for H_o=0.08 m. (a) U_g=1.0, and (b) 1.40 m/s.

The simulation results of solid volume fraction predicted at the bottom section of the conical bed (especially at *z*=0.05 m) by using Gidaspow [21] drag model were significantly lower than the experimental data. This discrepancy is attributed to the agglomeration of fine particles because of weight and inter particle attractive forces (i.e., van deer Walls, electrostatic and liquid bridges), especially at high particles loading [5,9]. Comparing the experimental measurement for the void fraction to that computed directly from the Gidaspow [21] drag model shows good agreement in the upper section of the bed (*z*=0.4 m).

Fig. 6 shows the radial dimensionless distribution curves of mean solid volume fraction in a conical fluidized bed for the particles loading of 0.10 m, with an inlet air velocity of 1.0 m/s (Fig. 6a) and 1.4 m/s (Fig. 6b).

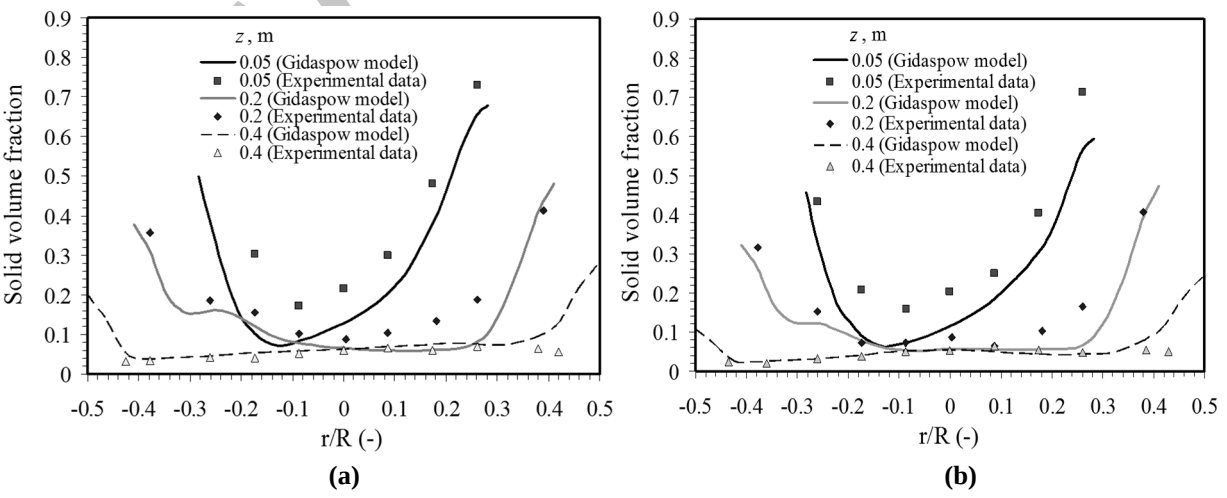

Figure 6. Radial distribution of solid volume fraction at H_o=0.10 m. a) U_g=1.0 and b) 1.4 m/s.

Table 3 shows the mean standard deviation between the experimental data and simulation results of solid volume fraction obtained by Gidaspow [21] drag model and applying partial-slip BC. The mean standard deviations in the spout zone for particles loading of 0.08 and 0.10 m are 15.2% and 20.1%, respectively, with an air velocity of 1.4 m/s, while these values were 6.47%, 7.86% and 11.45%, for particles loading of 0.012, 0.050 and 0.060 m, respectively [14,20]. This is explained by the fact that weight and inter particle forces are more severe as the static bed height of TiO_2 particles is higher and, therefore, the highest deviations between experimental data and simulation results are found at the maximum particles loading studied corresponding to 0.10 m. Thus, it can be found that, when a particles loading is twice (from 0.05 to 0.10 m), it causes a more than 150% increase in the value of mean standard deviation.

Fig. 7 shows the radial dimensionless distribution curves of the axial solid velocity obtained by using Gidaspow drag model for the particles loading of 0.08 m with an air velocity of 0.9 and 1.4 m/s. The air velocity has a distinct effect on the particle velocity in the spout zone but slight effect in the annular zone. This consequence differs from the results obtained by He and co-workers in case of spouted beds [26-27]. They found that the particle velocity in the annular zone increased with an increase in the inlet air velocity. The differences probably arise from the fact that the particle velocity in the annular zone of conical fluidized bed is fairly slow, as a result, its variation with air velocity is too little. Fig. 7 compares the results of model predictions with the experimental data. The simulations of axial solid velocity relatively match the experimental data at $|r/R| \geq 0.3$, but they were considerably higher than that of the experimental data, especially at the spout zone ($-0.05 \leq r/R \leq 0.05$).

Fig. 8 shows the radial dimensionless distribution curves of the axial solid velocity obtained by using Gidaspow drag model for the particles loading of 0.10 m with an air velocity of 0.9 and 1.4 m/s. With comparison of the results of Fig. 6-7a, it can be seen that the simulated axial solid velocity for H_o=0.1 m fluctuates more than those of H_o=0.08 m and does not show a full fluidization state. This shows that the model has predicted the heterogeneous behavior at high particles loading. However, the bed reaches to a relative full fluidization state at high gas velocities (Fig. 8b).

Table 3
Mean standard deviation between experimental data and simulation results of solid volume fraction of high particles loading of conical bed.

U_g (m/s)	Mean standard deviation (%)			
	H_o =0.08 m		H_o =0.10 m	
	Spout zone	Other zones	Spout zone	Other zones
1.0	16.5	13.6	23.5	15.0
1.4	15.2	13.0	20.1	13.7

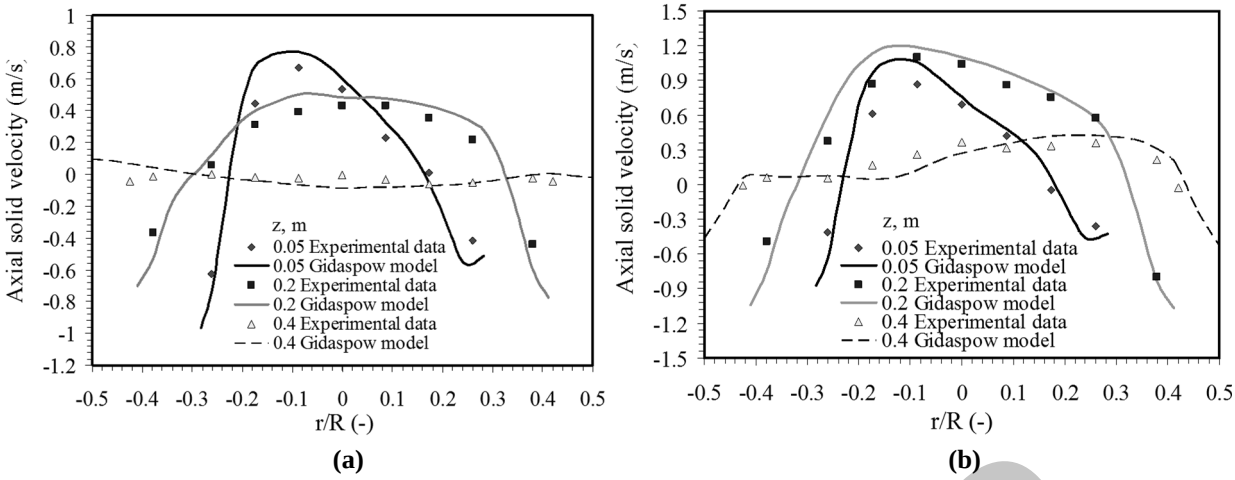

Figure 7. Radial distribution of axial solid velocity for H_o=0.08 m. a) U_g=0.9 m/s, b) U_g=1.4 m/s.

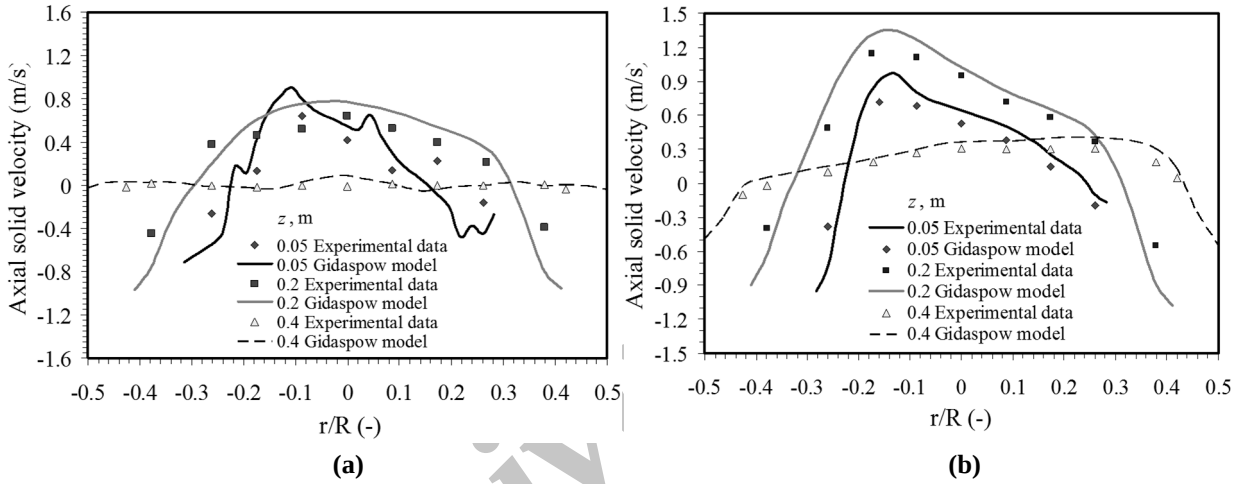

Figure 8. Radial distribution of axial solid velocity for H_o=0.10 m. a) U_g=0.90 m/s, b) U_g=1.40 m/s.

Increasing the particles loading at a fixed superficial air velocity tended to reduce the centralized airflow and spread the air out over the bed cross-section. Observation results show this spreading trend of the air with increased particles loading. In addition, the major flow resistance comes from inside of the solid particles and over their interface, therefore, the airflow becomes more centrally concentrated in the core of the bed and bubble formation in the denser annular region was suppressed when particles loading increased and the bed behavior was relatively close to spouted bed, especially at low air velocity.

Table 4

Mean standard deviation between experimental data and simulation results of axial solid velocity of high particles loading of conical bed.

U_g (m/s)	Mean standard deviation (%)			
	H_o =0.08 m		H_o =0.10 m	
	Spout zone	Other zones	Spout zone	Other zones
0.9	15.8	13.1	22.6	14.0
1.4	13.2	11.6	17.1	12.8

Table 4 shows the mean standard deviation between the experimental data and simulation results of axial solid velocity obtained by Gidaspow [21] drag model. The predictions were typically in greater agreement near the wall than the spout zone and spout-annular interface as the particle velocity is at its maximum in these zones. The highest deviations between the experimental and simulation results are found at high particles loading, corresponding to H_o=0.10 m, this is explained by the fact that, in experiments, increasing TiO_2 particles loading causes more agglomeration of particles and change in the local solid velocity in the bed and as a result more deviations. It can be seen that a 13.2 % and 17.1 % increase in standard deviation in the spout zone with an air velocity of 1.4 m/s when the particles loading increase from 0.08 to 0.10 m, respectively.

4. Conclusions

The hydrodynamic characteristics of conical fluidized bed containing micrometric TiO_2 particles were investigated experimentally and numerically at different gas velocities. At first, the effect of high particles loading on the radial profiles of the solid volume fraction and axial solid velocity were obtained by using an optical fiber technique. Experimental observations showed that large particles at the bottom and middle of the bed and mainly near the wall regions could be made to behave like a cohesive powder by applying large interparticle attractive forces and weight. This adhesion between the particles, particle-wall friction and contact between particles with gas distributor plays an important role on the overall bed pressure drop and determination of the minimum fluidization velocity. The particle flow regime in the conical bed with high particles loading is relatively similar to spouted beds with formation of spout and annular zones at the center and near the wall, respectively. There is a transition regime from the packed bed to channeling or heterogeneous state and then to a homogenous one, the bed reaches to relative solid circulation when the superficial air velocity is sufficiently high. Therefore, in conical beds, the particle mixing behaviors are obviously changed with the increase of particles loading and air velocity. Numerical studies of the proposed two-fluid model with k-ε turbulent model were carried out consequently using three different drag models and boundary conditions in order to investigate the effects of particles loading in the bed. The main conclusion is that the drag function proposed by Gidaspow gives a better prediction than the Syamlal-O'Brien and Arastoopour drag models. Furthermore, the use of the partial-slip boundary condition (φ=0.5) in the simulations gives a lower value of mean standard deviation in determination of the minimum fluidization velocity compared to the free- or no-slip BC. A comparison between the experimental data and simulation results shows that the transition region including heterogeneous and homogenous state was, for the most part, unclear in all simulations. The highest deviations have been shown in the characteristic curves at particles loading of 0.010 m, which can be explained by increasing particles loading causing more agglomeration of TiO_2 fine particles. Both experimental data and numerical results show that the mean solid volume fraction decreases

with the height in the bed, which becomes zero at the top of the bed. Furthermore, the value of the solid volume fraction is high in the annular zone and sharply decreases at the spout-annulus interface. The solid volume fraction predicted by the Gidaspow drag model showed better agreement at the upper section than the deeper section of the high loaded bed. The axial solid velocity predictions showed relatively better agreement with experimental results than the solid volume fraction; however, both results show high deviation at the spout zone. In general, in addition to the hydrodynamic parameters such as air velocity, pressure, particle size and density, the particles loading is an important parameter to estimate flow regime of the micrometric particles under fluidization for operational design and scale-up of conical fluidized beds.

Nomenclature

B slip coefficient, dimensionless
Bo_g granular bond number, dimensionless
C_D drag coefficient, dimensionless
$C_{1\mu}$, $C_{1\varepsilon}$, $C_{2\varepsilon}$, $C_{3\varepsilon}$=constants in the gas turbulence model, dimensionless
d_i inlet diameter, m
$d_{p,\,avg}$ average particle diameter, m
e_{ss} Restitution coefficient, dimensionless
g acceleration due to gravity, m.s^{-2}
$g_{0,ss}$ radial distribution coefficient, dimensionless
h total height of column, m
H_o initial particles loading, m
P Pressure, N.m^{-2}
R,r Radius, m
Re Reynolds number, dimensionless
t time, s
U,u gas velocity, m.s^{-1}
V particle velocity, m.s^{-1}
X weight fraction, dimensionless
z height from the bottom of the vessel, m

References

[1] Olazar, M., San Jose, M. J., Zabala, G. and Bilbao, J., "A new reactor in jet spouted bed regime for catalytic polymerizations", *Chem. Eng. Sci*., **49** (24), 4579 (1994).

[2] Hematian, S. and Faramarz Hormozi, F., ". Drying kinetics of coated sodium percarbonate particles in a conical fluidized bed dryer", *Powder Technol*., **269** (1), 30 (2015).

[3] Kmiec, A., "Hydrodynamics of flow and heat transfer in spouted beds", *Chem. Eng. J*., **19** (3), 189 (1980).

[4] Olazar, M., Aguado, R., Bilbao, J. and Barona, A., "Pyrolysis of sawdust in a conical spouted bed contactor with a HZSM-5 catalyst", *AIChE. J*., **46** (5), 1025 (2000).

[5] Zhou, T. and Li, H., "Estimation of agglomerate size for cohesive particles during fluidization", *Powder. Technol*., **101** (1), 57 (1999).

[6] Molerus, O., "Interpretation of Geldart's type A, B, C and D powders by taking into account interparticle cohesion forces", *Powder Technol*., **33** (1), 81 (1982).

[7] Wang, X. S., Rahman F. and Rhodes M. J., "Nanoparticle fluidization and Geldart's classification", *Chem. Eng. Sci*., **62** (1), 3455 (2007).

[8] Liu, J., Grace, J. R., and Bi, X., "Novel multifunctional optical-fiber probe: I. development and validation", *AIChE. J*., **49** (6), 1405 (2003).

[9] Pugsley, T., Chaplin, G. and Khanna, P., "Application of measurement techniques to conical Lab-scale fluidized bed dryers

containing pharmaceutical", *Trans. IChem. E*, **85** (3), 273 (2007).

[10] Pantzali, M. N., De Ceuster, B. Marin, G. B. and Heynderickx, G. J., "Three-component particle velocity measurements in the bottom section of a riser", *Int. J. Multiphase Flow*, **72** (1), 145 (2015).

[11] Li, J. and Kuipers, J. A. M., "Effect of pressure on gas-solid flow behavior in dense gas-fluidized beds; a discrete particle simulation study", *Powder Technol*., **127** (2), 173 (2002).

[12] Gidaspow, D., "Hydrodynamics of fluidization using kinetic theory: an emerging paradigm?", Recent Res. Devel. *Chem. Eng. Sci*., **5** (2-3), 53 (2003).

[13] Mostafa, A. A. and Mongia, H. C., "Investigation of Some Effective Parameters on the Fluidized Bed Grain Dryers", Iranica *J. Energy & Environm*., **4** (4), 391 (2013).

[14] Bahramian, A. and Olazar, M., "Profiling solid volume fraction in a conical bed of dry micrometric particles: Measurements and numerical implementations", *Powder. Technol*., **212** (1), 181 (2011).

[15] Van Wachem, B. G. M., Schouten, J. C., van den Bleek, C. M. and Sinclair, J. L., "Comparative analysis of CFD models of dense gas-solid systems", *AIChE. J*., **47** (5), 1035 (2001).

[16] Almuttahar, A. and Taghipour, F., "Computational fluid dynamics of high density circulating fluidized bed riser: study of modeling parameters", *Powder Technol*., **185** (1), 11 (2008).

[17] Benyahia, S., Syamlal, M. and O'Brien, T.J., "Evaluation of boundary conditions used to model dilute, turbulent gas/solids flows in a pipe", *Powder Technol*., **156** (2-3), 62 (2005).

[18] Johnson, P. C. and Jackson, R., "Frictional-collisional constitutive relations for granular materials, with application to plane shearing", *J. Fluid Mech*., **176** (1), 67 (1987).

[19] Hosseini, S. H., Ahmadi, G., Rahimi, R., Zivdar, M. and Nasr Esfahany, M., "CFD studies of solids hold-up distribution and circulation patterns in gas-solid fluidized beds", *Powder Technol*., **200** (3), 202 (2010).

[20] Bahramian, A., Olazar, M. and Ahmadi, G., "Effect of slip boundary conditions on the simulation of microparticle velocity fields in a conical fluidized bed", *AIChE. J*., **59** (12), 4502 (2013).

[21] Gidaspow, D., "Multiphase flow and fluidization", First ed., Academic press, London., (1994).

[22] Syamlal, M. and O'Brien, T. J., "Computer simulation of bubbles in a fluidized bed", *AIChE. Symp. Ser*., **85**, 22 (1989).

[23] Arastoopour, H., Pakdel, P. and Adewumi, M., "Hydrodynamics analysis of dilute gas-solid flow in a vertical pipe", *Powder Technol.*, **62** (2), 163 (1990).

[24] Geldart, D., "Types of gas fluidization," *Powder Technol*., **7** (5), 285 (1973).

[25] Schaeffer, D. G., "Instability in the evolution equations describing incompressible granular flow", *J. Diff. Eq*., **66** (1), 19 (1987).

[26] He, Y. L., Lim, C. J., Grace, J. J. R. and Qin, S. "Spout diameters in full and half spouted beds", *Can. J. Chem. Eng*., **76** (4), 702 (1998).

[27] Hagemeier, T., Börner, M., Bück, A. and Evangelos Tsotsas, E., "A comparative study on optical techniques for the estimation of granular flow velocities", *Chem. Eng. Sci*., **131** (1), 63 (2015).

Appendix A

The k-ε turbulence model, constants and parameters are presented in Table A.

Table A. *k-ε* Turbulence model, constants and parameters.

Turbulence kinetic energy (*k*)

$$\alpha_g \rho_g \left[\frac{\partial k}{\partial t} + \vec{U}_{g,j} \frac{\partial k}{\partial x_j} \right] = \frac{\partial}{\partial x_i} \left(\alpha_g \frac{\mu_{t,g}}{\sigma_k} \frac{\partial k}{\partial x_i} \right) + \alpha_g \tau_{g,ij} \frac{\partial \vec{U}_{g,i}}{\partial x_j} - \alpha_g \rho_g \varepsilon_g + \Pi_{k,g} \tag{A.1}$$

Turbulence dissipation rate (ε)

$$\alpha_g \rho_g \left[\frac{\partial \varepsilon}{\partial t} + \vec{U}_{g,j} \frac{\partial \varepsilon}{\partial x_j} \right] = \frac{\partial}{\partial x_i} \left(\alpha_g \frac{\mu_{t,g}}{\sigma_\varepsilon} \frac{\partial \varepsilon}{\partial x_i} \right) + \alpha_g \frac{\varepsilon}{k} \left(C_1 \tau_{g,ij} \frac{\partial \vec{U}_{g,i}}{\partial x_j} - C_2 \rho_g \varepsilon \right) + \Pi_{\varepsilon,g} \tag{A.2}$$

where σ_k and σ_ε are the turbulence Prandtl number for k and ε, respectively.

Appendix B

Governing and constitutive equations for Gas/Solid flows are presented in Table B.

Table B. Governing and constitutive equations for Gas/Solid Flows.

Continuity equation for phase i ($i = g$ for gas and s for solids)

$$\frac{\partial}{\partial t}(\alpha_i \rho_i) + \nabla.(\alpha_i \rho_i \vec{\mathbf{v}}_i) = 0 \tag{B.1}$$

Momentum conservation equation for gas and solid phase

$$\frac{\partial}{\partial t}(\alpha_g \rho_g \vec{\mathbf{U}}_g) + \nabla.(\alpha_g \rho_g \vec{\mathbf{U}}_g \vec{\mathbf{U}}_g) = -\alpha_g \nabla P + \nabla.\bar{\bar{\tau}}_g - \beta(\vec{\mathbf{U}}_g - \vec{\mathbf{v}}_s) + \alpha_g \rho_g \vec{\mathbf{g}} \tag{B.2}$$

$$\frac{\partial}{\partial t}(\alpha_s \rho_s \vec{\mathbf{v}}_s) + \nabla.(\alpha_s \rho_s \vec{\mathbf{v}}_s \vec{\mathbf{v}}_s) = -\alpha_s \nabla P + \nabla.\bar{\bar{\tau}}_s - \nabla P_s + \beta(\vec{\mathbf{U}}_g - \vec{\mathbf{v}}_s) + \alpha_s \rho_s \vec{\mathbf{g}} \tag{B.3}$$

Granular temperature conservation for solid phase

$$\frac{3}{2}\left[\frac{\partial}{\partial t}(\alpha_s \rho_s \theta_s) + \nabla.(\alpha_s \rho_s \theta_s \vec{\mathbf{v}}_s) \right] = -(P_s \bar{\bar{\mathrm{I}}} + \alpha_s \bar{\bar{\tau}}_s) : \nabla.\vec{\mathbf{v}}_s - \nabla.(\mathrm{k}_{\theta s} \nabla \theta_s) - \gamma \theta_s + \phi_{gs} \tag{B.4}$$

Solid stress-strain tensor

$$\bar{\bar{\tau}}_s = \mu_s \left(\nabla \vec{\mathbf{v}}_s + (\nabla \vec{\mathbf{v}}_s)^T \right) + \left(\lambda_s - \frac{2}{3}\mu_s \right) \nabla.\vec{\mathbf{v}}_s \tag{B.5}$$

Appendix C

The specularity coefficient, φ, is a measure of the fraction of collisions which transfers momentum to wall and varies from zero (free-slip condition or smooth walls) to one (no-slip condition or rough walls).

Table C. Johnson and Jackson semi-empirical equations [18].

Tangential velocity

$$v_{s,w} = -B\frac{\partial v_{s,w}}{\partial n} \qquad (C.1)$$

Slip coefficient

$$B = \frac{6\alpha_s.\mu_s}{\sqrt{3}\sqrt{\theta}.\pi.\varphi.\rho_s\, g_{0,ss}} \qquad (C.2)$$

Appendix D

The Syamlal-O'Brien, Arastoopour and Gidaspow drag models and the corresponding correlations of β to be investigated in this study are summarized in the Table D.

Table D. Drag models studied in this work

Syamlal - O'Brien (1988)

$$\beta = \frac{3}{4}\frac{C_D}{f^2}\frac{\rho_g\left|\bar{v}-u\right|}{d_P}\alpha_s\alpha_g \qquad (D.1)$$

where f is the ratio of the solid velocity to the terminal velocity of a single particle.

Arastoopour et al. (1990)

$$\beta = \left[\frac{17.3}{\mathrm{Re}_P} + 0.336\right]\frac{\rho_g}{d_P}\left|\bar{v}-u\right|\alpha_s\alpha_g^{-2.8} \qquad \mathrm{Re}_P = \frac{d_P\left|\bar{v}-u\right|\rho_g}{\mu_g} \qquad (D.2)$$

Gidaspow (1994)

$$\begin{cases} \beta_{Ergun} = 150\dfrac{\alpha_s^2\mu_g}{\alpha_g d_P^2} + 1.75\dfrac{\alpha_s\rho_g}{d_P}\left|V-U\right|, & \alpha_g < 0.8 \\ \beta_{Wen-Yu} = \dfrac{3}{4}C_D\dfrac{\alpha_s\rho_g}{d_P}\left|V-U\right|\alpha_g^{-2.65}, & \alpha_g \geq 0.8 \end{cases}$$

$$\beta = (1-\varphi_{gs})\beta_{Ergun} + \varphi_{gs}\beta_{Wen-Yu} \qquad (D.3)$$

$$\begin{cases} C_D = \dfrac{24}{\mathrm{Re}_{P1}}[1+0.15(\mathrm{Re}_{P1})^{0.687}], \mathrm{Re}_p < 1000 \\ C_D = 0.44, \mathrm{Re}_p \geq 1000 \end{cases}$$

$$\mathrm{Re}_p = \frac{\alpha_g\rho_g\left|\bar{v}-u\right|d_P}{\mu_g}$$

$$A = \alpha_g^{4.14}$$

$$\begin{cases} B = \alpha_g^{2.65}, \alpha_s < 0.15 \\ B = 0.8\alpha_g^{1.28}, \alpha_s \geq 0.15 \end{cases}$$